Machine Learning Based Visible Light Indoor Positioning With Single-LED and Single Rotatable Photo Detector

Ren Liu, Zhonghua Liang, *Senior Member, IEEE*, Kuo Yang, and Wei Li, *Member, IEEE*

***Abstract*—In recent years, visible light positioning (VLP) systems have attracted considerable attention because they do not require additional infrastructures. However, most existing researches on the VLP ignore the impact of wall diffuse reflection, which can lead to the dramatical decrease of the position accuracy performance near the indoor walls and corners. In this paper, we design an indoor VLP system with one single light-emitting diode (LED) and a rotatable photodetector (PD), and then propose an indoor VLP algorithm based on machine learning (ML) methods with concern for the indoor reflection of the optical propagation. The proposed positioning process is implemented via two stages: area classification and positioning. During the area classification stage, by using the random forest (RF) algorithm, the entire room is divided into one interior area and four wall or corner zones. In the interior area, the rotatable PD is directly used to determine the target location. In the four wall or corner zones, a hybrid positioning algorithm based on the extreme learning machine (ELM) and the density-based spatial clustering of applications with noise (DBSCAN) is developed to improve localization accuracy near the indoor walls and corners. Simulation results show that by using the proposed indoor VLP system with the rotatable PD and the hybrid algorithm, the maximum and averaged positioning errors of wall or corner zones drop from 137.96 cm and 15.63 cm, to 38.34 cm and 1.43 cm, respectively, and the averaged positioning error of the whole room decreases from 11.97 cm to 1.74 cm.**

***Index Terms*—Density-based spatial clustering of applications with noise (DBSCAN), extreme learning machine (ELM), Internet of things (IoT), random forest (RF), rotatable PD, single LED, visible light positioning (VLP).**

I. Introduction

In RECENT years, with the blooming of Internet of Things (IoT) technologies [1], there have been gradually increased requirements for the various services based on the location information. In outdoor environments, GPS or Beidou navigation equipment can achieve accurate positioning [2]. However, the indoor GPS signal could be weak or even be blocked due to the loss of satellite signals by obstructions from buildings and it leads to low positioning accuracy [3]. Therefore, the more reliable positioning systems are needed for indoor environments [4]. Traditional indoor positioning techniques, such as WLAN, UWB, and Bluetooth [5], [6], require additional infrastructures [7]. Meanwhile, they are easy to cause electromagnetic signal interference [8], and thus they are not suitable for the applications which are sensitive to electromagnetic signal interference. Recently, the visible light communication (VLC) has become one of the essential techniques for the oncoming 6G wireless communications [9]. Therefore, the visible light positioning (VLP) based on the VLC has become a promising technology in the field of the indoor positioning thanks to its inherent advantages, such as no requirements to deploy additional infrastructures, low cost, and long service life [10], [11].

Most of the existing VLP systems are based on multiple light-emitting diodes (LEDs) and they exploit TDMA [12], FDMA [13] or CDMA [14] technologies to avoid the mutual interference among LEDs. In addition, these positioning systems with multi-LED usually have high hardware complexity and high cost. In contrast, the use of VLP system with single-LED can avoid mutual interference among LED lights, the influence of the multi-LED layout on positioning accuracy, and the waste of LED light resources. Therefore, the VLP technology with single-LED is more practical and it is more energy-efficient especially for a small room [2].

In recent years, the various VLC/VLP systems based on the received signal strength (RSS) have been developed, in which machine learning (ML) algorithms are widely employed, such as the artificial neural network (ANN) [15], the convolutional neural network (CNN) [16], the density-based spatial clustering of applications with noise (DBSCAN) [17], the ridge regression (RR) [18], and the extreme learning machine (ELM) [19]. These VLC/VLP systems have relatively better positioning performance. However, most of them require a large number of iterations for training the network, which lead to the higher computational complexity.

In the indoor VLP technologies, the optical receivers are generally comprised of photo detectors (PD) and image sensors. For the single-LED positioning technologies, the receivers equipped with multiple PDs are designed in [20], [21], and the image sensors with high resolution are exploited to obtain position parameters in [5], [22], [23]. However, recent achievements in high-precision angle sensors have paved the

Manuscript received January 9, 2022; revised February 22, 2022; accepted March 25, 2022. Date of publication March 30, 2022; date of current version April 18, 2022. This work was supported in part by the Natural Science Basic Research Project in Shaanxi Province of China under Grant 2020JM-242, in part by the National Natural Science Foundation of China under Grant 61871314, and in part by the Fundamental Research Funds for the Central Universities, CHD under Grant 300102249303. *(Corresponding author: Zhonghua Liang.)*

The authors are with the Department of Communication Engineering, School of Information Engineering, Chang'an University, Xi'an, Shaanxi 710064, China (e-mail: 2019124004@chd.edu.cn; lzhxjd@hotmail.com; 17865519557@163.com; wli.chd@chd.edu.cn).

Digital Object Identifier 10.1109/JPHOT.2022.3163415

way for the development of the single-PD positioning systems. In this paper, we investigate the VLP system with single-LED and single-PD [24], [25] where a rotatable PD measures the relative angles with respect to the LED projection point as well as the maximum or minimum RSS values. In practice, such a VLP system can be a smart phone equipped with a compass or a robot equipped with a motor rotating at a constant speed. The horizontal distance between the platform and the LED projection point is obtained by the measured RSS value. Our major contributions are summarized as follows:

1) Firstly, the random forest (RF) classification algorithm is introduced to the VLP system so as to divide the measured room into two parts: one interior area and four wall or corner zones. For the interior area, the location of target node (TN) can be directly determined ONLY based on the relative angle and the horizontal distance measured by the rotatable PD.
2) For the four wall or corner zones, a hybrid positioning algorithm based on the ELM and DBSCAN methods is proposed, in which the trained ELM is firstly employed to each wall or corner zone to obtain an estimation of the target coordinates. Meanwhile, the rotatable platform will be moved in a small area to re-estimate the coordinates for some singular points and the DBSCAN algorithm is used to find the largest cluster of TN estimated coordinates and weight the largest cluster to improve the positioning accuracy.

It is worth noting that although the same ELM algorithm is investigated for the VLP systems in both [19] and our work, there are still two significant differences between them as follows:

Firstly, in [19], the original ELM algorithm and fingerprinting are both employed in entire measured room to obtain an estimation of the TN's location. However, in our work, the proposed hybrid ELM-DBSCAN algorithm is ONLY used for four wall or corner zones to improve the positioning accuracy, and for the interior area, ONLY the use of the rotatable positioning model with single rotatable PD is sufficient to determine the TN's location. By this means, when the RF classification algorithm is used to roughly estimate that the TN's location belongs to the interior area, it will make sense to reduce the computational complexity without significant loss in localization accuracy.

Secondly, in the ELM algorithm used in [19], the number of input parameters, namely the received power values, depends on the number of LEDs, which is strictly limited by hardware complexity and cost. In our work, since the power value received from any angle can be captured by the rotatable PD, the number of inputs can be flexibly selected according to the accuracy requirements.

The rest of this paper is organized as follows. In Section II we present the background including system model, noise model and the machine learning algorithms used in this paper. Then we describe the rotatable VLP positioning model and the proposed hybrid positioning algorithm in Section III. Furthermore, simulation results are given in Section IV to demonstrate the effectiveness of the proposed VLP algorithm. Finally, conclusions are summarized in Section V.

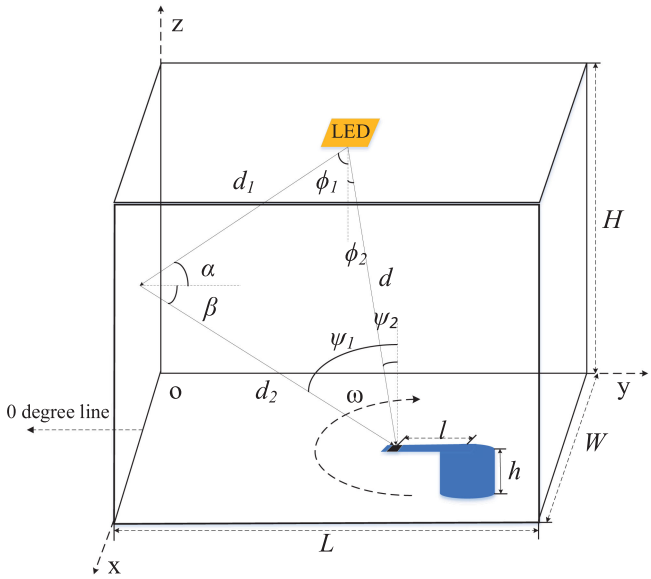

Fig. 1. Indoor VLP system with single-LED and single rotatable PD.

II. Background

A. System Model

We consider an indoor scenario with single-LED illumination. Fig. 1 illustrates the indoor VLP system with single-LED and single rotatable PD. The modulated optical signal is transmitted by the LED light installed at the center of the roof, and the rotatable platform (with blue highlighting) detects and demodulates the received optical signal. The rotatable platform includes a cylindrical body centered on the position of TN, and a rotating arm equipped with an angle sensor and the PD. When viewed from above, the horizontal arm rotates clockwise.

When the visible light signal is transmitted indoors, it is easy to be reflected by indoor facilities or walls, and thus there appears multiple reflection signals which can decrease the position accuracy. In this paper, we assume that the first order non-line-of-sight (NLOS) component dominates all NLOS reflection components, which is one of typical cases for indoor VLC or VLP channel modeling reported in [26].[1]

We assume that the propagation of visible light in space follows the Lambert radiation model, in which the order of Lambert emission m and the channel DC gain $H(0)$ can be given as follows [29]:

$$m = \frac{-ln2}{ln(\cos\phi_{1/2})}, \tag{1}$$

$$H(0) = \begin{cases} \frac{(m+1)A}{2\pi d^2} F_1(\phi_2, \psi_2) & 0 \le \psi_2 \le \psi_c \\ 0 & \psi_2 > \psi_c, \end{cases} \tag{2}$$

where $F_1(\phi_2, \psi_2) = \cos^m(\phi_2) T_s(\psi_2) g(\psi_2) \cos(\psi_2)$, $\phi_{1/2}$ is the half power angle of the LED, A represents the active area

[1]Such an assumption does not represent all typical indoor VLC or VLP scenarios because there should be other typical cases for indoor VLC or VLP channel modeling, such as those presented in [27] and [28].

of the PD at the receiver, d is the distance between the LED and the PD, ϕ_2 and ψ_2 denote the angle of irradiance and the angle of incidence between the LED and the PD, respectively (When the PD is placed horizontally, ϕ_2 and ψ_2 are equal). ψ_c represents the field-of-view of the receiver. $T_s(\psi)$ is the gain of an optical filter, $g(\psi)$ is the gain of an optical concentrator, which is expressed as [30]:

$$g(\psi) = \frac{n^2}{\sin^2 \psi_c}, \tag{3}$$

where n is the refractive index. For convenience of expression, we only consider the reflection of walls and therefore the DC gain of a primary reflection from a reflective surface of area dA is given by [31]:

$$H_{re}(0) = \begin{cases} \frac{(m+1)A}{2\pi^2 d_1^2 d_2^2} \rho \cos^m(\phi_1) F_2(\alpha, \beta, \psi_1) & 0 \le \psi_1 \le \psi_c \\ 0 & \psi_1 > \psi_c, \end{cases} \tag{4}$$

where $F_2(\alpha, \beta, \psi_1) = d_A \cos(\alpha) \cos(\beta) T_s(\psi_1) g(\psi_1) \cos(\psi_1)$, d_1 represents the distance from the LED to the reflection point, d_2 is the distance between the reflection point and the PD, ρ is the reflection factor, d_A denotes the reflection area, ϕ_1 and α respectively indicate the irradiance angle and incident angle of the reflection point, respectively. β and ψ_1 are the irradiance angle and incident angle of the PD, respectively.

The optical power received by the PD can be calculated as:

$$P_{opt} = P_t \times \left[H(0) + \sum_{j=1}^{4} \sum_{i=1}^{m_j} H_{re}^{ij}(0) \right], \tag{5}$$

where P_t is the optical emission power, j and m_j are the identification(ID) number of walls and the total number of reflectors with area d_A on the j-th wall, respectively. $H_{re}^{ij}(0)$ represents the DC gain of the primary reflection from the i-th reflecting surface of the j-th wall.

B. Noise Model

In the VLP system, the noise usually can be divided into two parts: thermal noise and shot noise. Thermal noise mainly includes feed-back impedance noise and field effect pipe noise. Shot noise is mainly related to background current originated from background light or sunlight. The electrical power received by the PD includes the electrical power converted from optical power and the noise power, and thus it can be defined as [25]:

$$P_{el} = (R_p \times P_{opt})^2 + \delta_{noise}^2, \tag{6}$$

where R_p denotes the PD responsiveness. δ_{noise}^2 is the sum of the variances of shot noise and thermal noise, and it can be expressed as:

$$\delta_{noise}^2 = \delta_{shot}^2 + \delta_{thermal}^2. \tag{7}$$

The variance of shot noise δ_{shot}^2 can be obtained from [32]:

$$\delta_{shot}^2 = 2qR_p P_{opt} B + 2qI_{bg} I_2 B, \tag{8}$$

where I_{bg} is dark current generated by background light, q denotes electronic charge, I_2 indicates noise bandwidth factor, B represents equivalent noise bandwidth.

The variance of thermal noise $\delta_{thermal}^2$ is given by [32]:

$$\delta_{thermal}^2 = \frac{8\pi k T_k}{G} C_{pd} A I_2 B^2 + \frac{16\pi^2 k T_k \Gamma}{g_m} C_{pd}^2 A^2 I_3 B^3, \tag{9}$$

where T_k is absolute temperature, k denotes Boltzmann's constant, C_{pd} represents the fixed capacitance of the photo detector per unit area, G is open-loop voltage gain, g_m denotes the FET transconductance, Γ is FET noise factor, I_3 is noise bandwidth impact factor.

C. Algorithms Investigated in This Paper

1) RF Classification Algorithm: The RF classification algorithm does not require too many parameters, and thus it can be used in different fields. Because this algorithm randomly selects data and features, it has good anti-noise performance without over-fitting.

The RF algorithm is a ML method based on integrated learning, in which multiple decision trees are used for each forest as training samples. Moreover, the new sample will be given a classification value. Then, the final classification result is obtained based on the principle that the minority obeys the majority. The voting decision process is given as [33], [34]:

$$H(x) = arg \max_{Y} \sum_{i=1}^{k} I(h_i(x) = Y), \tag{10}$$

where $H(x)$ represents a combined classification model, h_i is single decision tree, Y is the output variable and $I(\cdot)$ denotes indicator function. The implementation steps of the RF classification algorithm are provided in Appendix A.

2) ELM Algorithm: The ELM algorithm is a feed-forward neural network algorithm based on a single hidden layer, which has the advantages of fast learning speed and good generalization performance. Compared with the ELM, the traditional feed-forward neural network has a slow training speed and is easy to appear as a local minimum. Moreover, the ELM algorithm randomly generates the connection weights of the input layer to the hidden layer and the threshold of the hidden layer neurons. When using it, only the number of hidden layer neurons and the type of activation function need to be set to find the unique optimal solution. It can be used for classification and fitting of data [19], [34].

Suppose the given feedforward neural network has L hidden neurons and N training samples $(\mathbf{x}_i, \mathbf{y}_j)$, where $\mathbf{x}_i = [x_{i1}, x_{i2}, \ldots, x_{in}]^T \in R^n$ and $\mathbf{y}_i = [y_{i1}, y_{i2}, \ldots, y_{im}]^T \in R^m$, n and m are the numbers of input layer and output neurons.

Mathematical model of the ELM algorithm can be described as [35]:

$$f_L(x_j) = \sum_{i=1}^{L} \boldsymbol{\beta}_i g(\boldsymbol{\omega}_i x_j + \mathbf{b}_i) = \mathbf{y}_j, j = 1, 2, .., N, \tag{11}$$

where $\boldsymbol{\omega}_i = [\omega_{i1}, \omega_{i2}, \ldots, \omega_{in}]^T$, is the input weight from the input layer to the i-th hidden node, and $\boldsymbol{\beta}_i = [\beta_{i1}, \beta_{i2}, \ldots, \beta_{im}]^T$, represents the output weight from the i-th hidden node to the output layer and $\mathbf{b}_i$ denotes the bias of the i-th hidden node. $g(\cdot)$ refers to the activation function. (11) can be expressed in matrix form:

$$\mathbf{H}\boldsymbol{\beta} = \mathbf{Y}, \tag{12}$$

where

$$\mathbf{H} = \begin{bmatrix} g(\omega_1 x_1 + b_1) & g(\omega_2 x_1 + b_2) & \cdots & g(\omega_L x_1 + b_L) \\ g(\omega_1 x_2 + b_1) & g(\omega_2 x_2 + b_2) & \cdots & g(\omega_L x_2 + b_L) \\ \vdots & \vdots & \ddots & \vdots \\ g(\omega_1 x_N + b_1) & g(\omega_2 x_N + b_2) & \cdots & g(\omega_L x_N + b_L) \end{bmatrix}$$

$\boldsymbol{\beta} = [\boldsymbol{\beta}_1^T, \boldsymbol{\beta}_2^T, \ldots, \boldsymbol{\beta}_L^T]^T$, $\mathbf{Y} = [\mathbf{y}_1^T, \mathbf{y}_2^T, \ldots, \mathbf{y}_L^T]^T$, $\mathbf{H}$ represents the output matrix of the hidden layer neuron, $\mathbf{Y}$ is the expected output vector. Using the least square method, the ELM model is trained to find an estimated $\boldsymbol{\beta}$ minimizing the error, which can be calculated as:

$$\hat{\boldsymbol{\beta}} = \mathbf{H}^{+}\mathbf{Y}, \tag{13}$$

where $\mathbf{H}^{+}$ represents the generalized inverse of the matrix $\mathbf{H}$. The implementation process of the ELM algorithm is presented in Appendix B.

3) DBSCAN Algorithm: The DBSCAN algorithm is a density-based clustering algorithm. This clustering algorithm generally assumes that the category can be determined by the tightness of the sample distribution. Samples of the same category are closely connected to each other. In other words, there must be samples of the same type not far from any sample of that category.

Compared with the traditional K-means algorithm, the DBSCAN does not need to specify the number of categories. It can find clusters of any shape, and discover abnormal points while clustering, and is not sensitive to abnormal points in the data set. DBSCAN just needs to jointly adjust the two parameters: the distance threshold ε and the threshold of number of neighborhood sample $MinPts$, which have significant effect on the clustering performance [17]. The entire procedure of the DBSCAN algorithm is given in Appendix C.

III. VLP System

A. Rotatable Positioning Model

In the designed rotatable positioning platform with single-PD, it is assumed that the height of the positioning platform is constant. The positioning platform needs to obtain two parameters from the received signal by the PD: one is the horizontal distance from the PD to the LED projection point, and the other is the relative angle between the PD and the LED projection point with respect to the zero-degree line [24]. The principle of rotatable positioning model is shown in Fig. 2. In Fig. 2, D_h refers to the horizontal distance between the PD and the LED projection point (the yellow pentagram), and it can be defined as:

$$D_h = \sqrt{d^2 - (H - h)^2}, \tag{14}$$

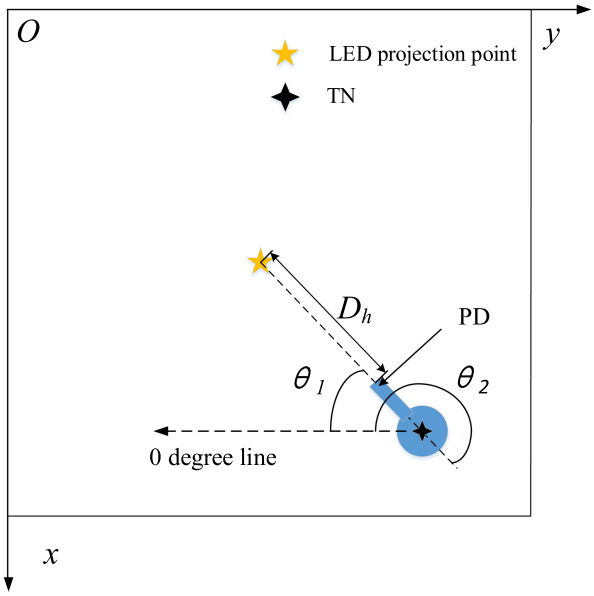

Fig. 2. Principle of the rotatable positioning model.

where d denotes the distance between the PD and the LED and it can be computed by the RSS values, H is the height of the room, and h refers to the height of rotatable platform as shown in Fig. 1.

The PD rotates clockwise along the zero-degree line with a constant angular velocity ω, and T is defined as the signal sampling interval of the PD. The power values of the electrical signal sampled by the PD in one rotation cycle can be described as:

$$\mathbf{P} = [P(0)\ P(\omega T)\{\ldots\}P(\omega n_1 T)], \tag{15}$$

where $n_1 + 1$ represents the number of the samples in one cycle.

When the PD rotates around the TN, the received optical power fluctuates with the varying distance from the LED to the PD. When the PD is facing the LED, the received power reaches the maximum with the relative angle $\theta = \theta_1$. Conversely, when the PD is facing away from the LED, the received power is the minimum with the relative angle $\theta = \theta_2$. From Fig. 2, we see that the absolute angle difference $|\theta_2 - \theta_1| = \pi$ in theory.[2] Therefore, θ_1 and θ_2 can be obtained by

$$\theta_1 = arg \max_{\theta = iT\omega} (\mathbf{P}) \tag{16}$$

and

$$\theta_2 = arg \min_{\theta = jT\omega} (\mathbf{P}), \tag{17}$$

respectively.

Using the obtained θ_1 and θ_2 values, the four coordinates of the TN can be obtained as:

$$x_1 = x_0 + (D_h + l)\sin\theta_1, \tag{18}$$

$$y_1 = y_0 + (D_h + l)\cos\theta_1, \tag{19}$$

[2]However, the measured value of the absolute angle difference may not be π in practice.

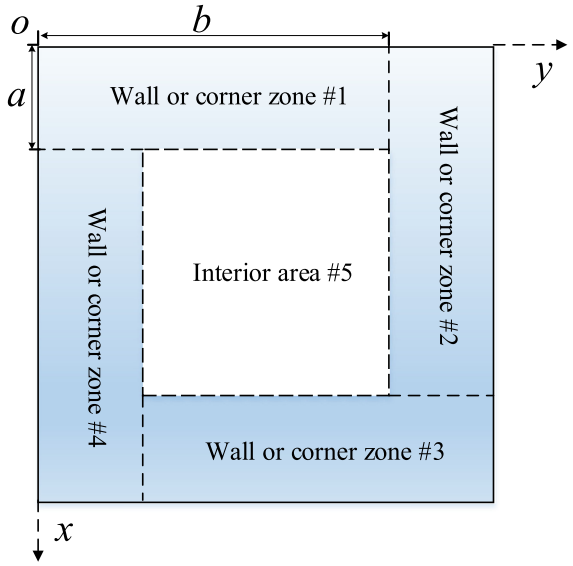

Fig. 3. Area classification with the hybrid positioning algorithm.

$$x_2 = x_0 - (D_h - l)\sin\theta_2, \tag{20}$$

$$y_2 = y_0 - (D_h - l)\cos\theta_2, \tag{21}$$

where (x_1, y_1) and (x_2, y_2) represent the estimated position coordinates of the TN, respectively. (x_0, y_0) denotes the coordinates of the LED projection point, and l refers to the length of the rotating arm. Therefore, the estimated position of the TN can be expressed as:

$$\hat{x} = (x_1 + x_2)/2, \tag{22}$$

$$\hat{y} = (y_1 + y_2)/2. \tag{23}$$

The positioning error can be recorded as:

$$E = \sqrt{(\hat{x} - x_{ture})^2 + (\hat{y} - y_{ture})^2}, \tag{24}$$

where (x_{ture}, y_{ture}) denotes the true location coordinates of the TN.

B. Proposed Hybrid Positioning Algorithm

Based on the above discussions, we see that even if the rotatable positioning model is used, the positioning error near the walls or corners will be still large since the impact of the wall diffuse reflection on the location accuracy should not be neglected. In order to tackle this problem, the measured room can be divided into two areas: interior area and wall or corner area. If the TN belongs to the interior area, the rotatable positioning model can be directly used. If the TN is located in the wall or corner area, the more efficient positioning algorithm can be developed to improve the positioning accuracy.

Moreover, in order to obtain high positioning accuracy, the wall or corner area can be further divided into four zones, each of which contains a corner of the room. Accordingly, as shown in Fig. 3, the entire room can be divided into five zones: four wall or corner zones $(\#1 - \#4)$, and the interior area $(\#5)$. In this paper, the RF classification algorithm is used to divide the whole room into five area or zones using the received power values from different angles and then roughly estimate which area or zone the TN belongs to.

Algorithm 1: Hybrid Positioning Algorithm.

Inputs: Initial L_1, $[\boldsymbol{\omega}_i, \mathbf{b}_i, \boldsymbol{\beta}_i]$, for $i = 1, 2, 3, 4$, N, ε, $MinPts$, $f(\cdot)$, $\mathbf{R} = \emptyset$, and c.

1: Received power $\mathbf{P}_1$=$[P_0, P_{60}, P_{120}, P_{180}, P_{240}, P_{300}]^T$;

2: Obtain the estimated $index$ by performing RF classification;

3: If $index = 5$, calculate $\mathbf{X}$ with rotatable positioning model. Otherwise, calculate $\mathbf{X}$ by ELM using $\mathbf{P}_1$ in $index$ subarea.

4: If $\mathbf{X}$ is in the area of Subarea ($index$), store $\mathbf{X}$ into $\mathbf{R}$, go to step 1, repeat L_1 times. Otherwise, move the position of the rotatable platform, go to step 1, repeat L_1 times;

5: If the number of elements of $\mathbf{R}$ is greater than or equal to c, perform clustering using DBSCAN;

a) If the result of step 5 is all noise, the clustering fails, $\boldsymbol{X} = [-1 - 1]^T$, jump back to step 1, $\mathbf{R} = \emptyset$.

b) Otherwise, select the cluster that contains the largest number of coordinates to estimate the weighted coordinates;

6: If the number of elements of $\mathbf{R}$ is less than c, $\boldsymbol{X} = [-2 - 2]^T$;

Outputs: Position of TN $\boldsymbol{X}$.

If the TN is estimated to be located in the interior area, the rotatable positioning model can be directly used to determine its coordinates. If the TN is estimated to be located in any of the four wall or corner zones, a hybrid algorithm based on the ELM and the DBSCAN is developed to estimate the coordinates of the TN position. The main idea of the hybrid algorithm can be explained as follows. The ELM algorithm is effective for determining most positions in the zone, except for a few singular points whose estimated positions drift across the boundary of the zone. When one or more singular points are detected, these singular points will be replaced by their adjacent perturbation points at random and this means re-moving the rotatable device to receive power in a small area. Theoretically, the coordinate points of the rotatable platform near the TN should be gathered together after being positioned by ELM. The DBSCAN algorithm can be used to find the coordinate points that are clustered together and find the largest number of clusters weighted to determine the location of TN.

Assuming that the largest cluster detected by the DBSCAN clustering algorithm contains M coordinates, they can be expressed as $\mathbf{C} = [(x_1, y_1), (x_2, y_2), \ldots, (x_M, y_M)]^T$. The centroid $(\bar{x}, \bar{y})$ of the coordinate set $\mathbf{C}$ can be given by:

$$(\bar{x}, \bar{y}) = \left(\frac{1}{M}\sum_{i=1}^{M} x_i, \frac{1}{M}\sum_{i=1}^{M} y_i\right). \tag{25}$$

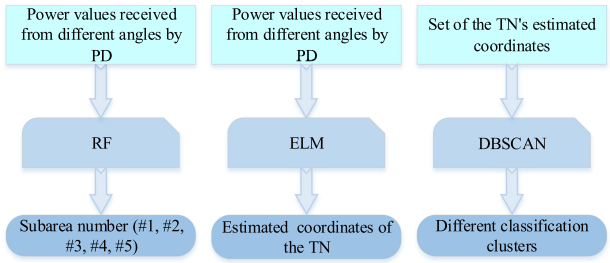

Fig. 4. Block diagram of the three machine learning algorithms used in this paper.

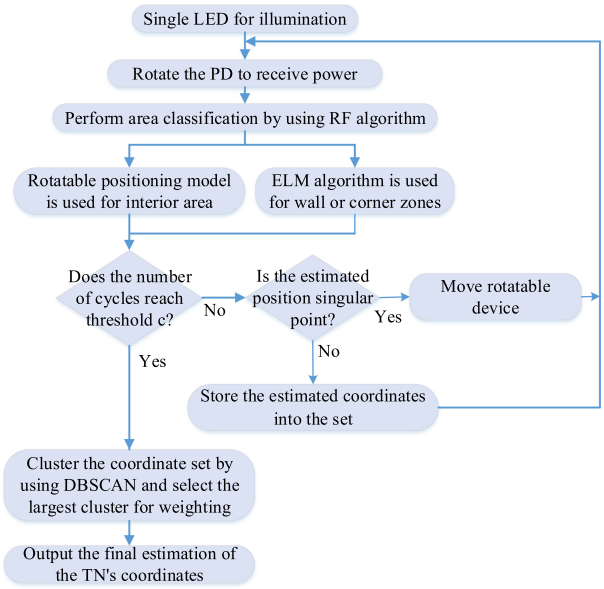

Fig. 5. Block diagram of the proposed hybrid positioning algorithm.

The Euclidean distance D from the points in the set to the centroid can be calculated as:

$$D_i = \sqrt{(x_i - \bar{x})^2 + (y_i - \bar{y})^2}, i = 1, 2, .., M. \tag{26}$$

The weight of each coordinate can be expressed as $\mathbf{K} = [k_1, k_2, .., k_M]$, where k_i for $i = 1, 2, \ldots, M$ is given as:

$$k_i = \frac{e^{-D_i}}{\sum_{i=1}^{M} e^{-D_i}}. \tag{27}$$

The final estimated coordinates $\mathbf{X}$ can be expressed as:

$$\mathbf{X} = \mathbf{KC}. \tag{28}$$

The block diagram of the proposed hybrid positioning algorithm and the input and input of the three machine learning algorithms used in this paper are shown in Fig. 5 and Fig. 4, respectively. In addition, the symbols used in the proposed hybrid positioning algorithm and the corresponding descriptions are provided in Table I. Finally, Algorithm 1 provides the implementation process of the hybrid ML positioning algorithm, in which $\boldsymbol{X} = [-1 - 1]^T$ and $\boldsymbol{X} = [-2 - 2]^T$ do not represent any actual position, where the former is used as a meaning of the clustering failed, and the latter is used as an indicator of error area-classification.

TABLE I
PARAMETER DESCRIPTION

Symbol	Description
$\mathbf{X}$	position of TN
L_1	number of estimated locations
N	number of decision trees in the RF
$f(\cdot)$	fitted electric power and slope distance equation
$\mathbf{R}$	set of estimated coordinates
Subarea(i)	wall or corner zone # i
c	minimum number of $\mathbf{X} \in$ Subarea(i) in $\mathbf{R}$
P_i	RSS at angle i compared to the zero-degree line

TABLE II
SIMULATION PARAMETER

Symbol	Description	Value
T_s	optical filter gain	1
n	refractive index	1.5
$d_A(m^2)$	area of reflecting surface	0.067
ρ	reflection factor	0.8
q	electronic charge	1.6×10^{-19}
$B(MHz)$	equivalent noise bandwidth	400
$I_{bg}(uA)$	dark current	5100
I_2	noise bandwidth factor	0.562
K	Boltzmann's constant	1.38×10^{-23}
T_k	absolute temperature	300
I_3	noise bandwidth impact factor	0.868
$g_m(mS)$	FET transconductance	30
$C_{pd}(pF/cm^2)$	fixed capacitance per unit area	112
G	open-loop voltage gain	10

IV. SIMULATION RESULTS

In order to evaluate the positioning performance of the proposed VLP system with single-LED and single rotatable PD based on the proposed rotatable positioning model and hybrid positioning algorithm, the computer simulations are carried out in a $4\,m \times 4\,m \times 3.1\,m$ indoor scenario using MATLAB platform. As shown in Fig. 1, the position coordinates of the LED light is set as (2,2,3.1), the height of the rotatable device $h = 0.1$ m, the length of the rotating arm $l = 0.05 \sim 0.20$ m, the emission power of the LED $P_t = 100$ W, the PD area $A = 10$ cm^2, the half power angle $\phi_{1/2} = 60°$, the PD's angle of view $\psi_c = 60°$, and the PD responsiveness $R_p = 0.54$ A/W. Because $l = 0.05 \sim 0.20$ m, the rotatable device cannot reach the area within $0.05 \sim 0.20$ m away from the wall, and thus this area is not considered in the simulation. Similar to the parameter settings presented in [26], [32], [36], some important parameters related to the system model and the noise model are provided in Table II.[3]

In order to train the RF and ELM algorithms, the training data is collected at 6 cm spaces in the different positions of

[3]It is noted that in this paper, we consider an indoor VLC system integrating lighting, communication and positioning functions, which has the potential to be a promising solution for future indoor VLC scenarios. In such a system, the date rate can reach several hundreds of megabits per second or higher, and thus the equivalent noise bandwidth can also reach hundreds of megahertz or more. Similarly, the equivalent noise bandwidth presented in [32] is as high as 800 MHz. Therefore, in Table II we set $B = 400$ MHz denoting a moderate equivalent noise bandwidth for the investigated VLC system.

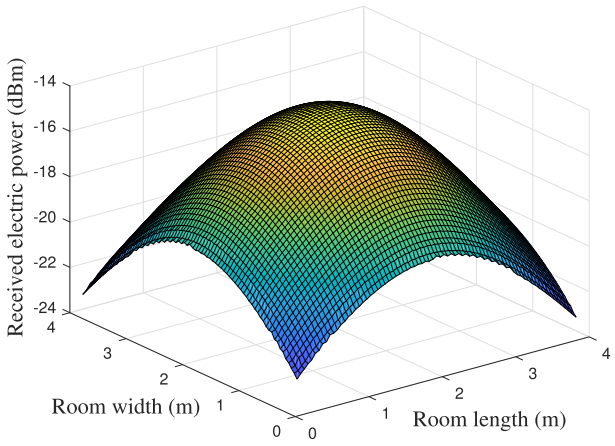

Fig. 6. Distribution of electrical power in the measured room.

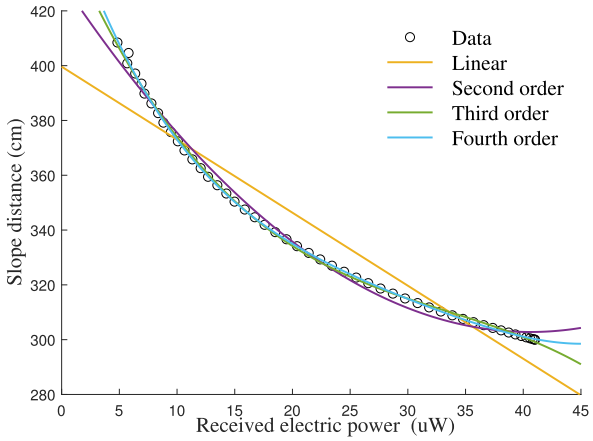

Fig. 7. Fitting results of polynomials with different order.

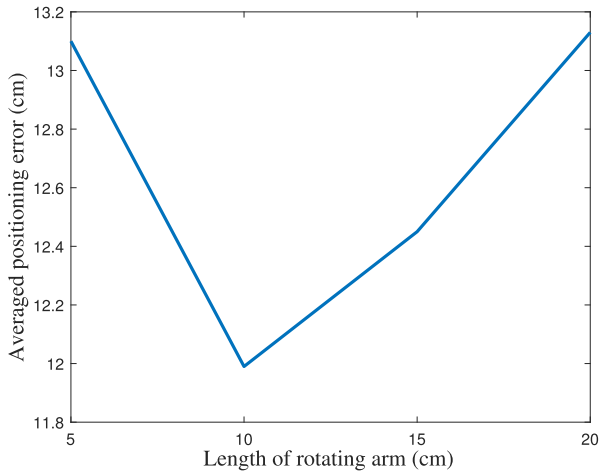

Fig. 8. Influence of the length of rotating arm on averaged positioning error of the rotatable positioning model.

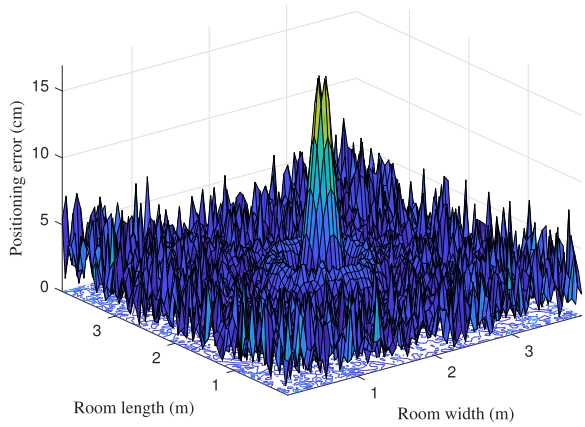

Fig. 9. Positioning error distribution of rotatable positioning model (LOS).

the room, and thus there are totally 4225 sets of data. Each training data set includes 6 electric power values received at integer multiples of 60-degree compared to 0° line respectively, 2 coordinate values of the TN, and the information about the target-affiliated zone. Moreover, the 6 electric power values are collected as a set of tested data at 5 cm spaces in the room, and thus there are are 5929 sets of tested data in total. Based on the collected electric power values, the ELM values in different regions are trained separately in different wall or corner zones. In addition, the activation function of ELM is set to $sigmoidal$ function and the number of hidden layer neurons is set to 200.

Fig. 6 shows the distribution of the received electrical power values in the PD. We see that the closer the position of the PD is to the center of the room, the greater the electrical power received by the PD. The maximum, minimum and average of the electrical power values are equal to -13.8698 dBm, -22.3297 dBm and -17.1502, respectively.

In order to demonstrate the relationship of the received electric power and the slope distance between PD and LED, we collected data every 4 cm along the diagonal of the room (from one corner to the projection point of the LED) and obtained totally 50 sets of data. Based on the obtained 50 sets of data, the fitting results of polynomials with different orders are shown in Fig. 7, we see that the degree of fitting increases with the order of the polynomial. When the order of the polynomial is 4, the degree of fitting can be satisfied. Therefore, in the following simulations, the highest order of the fitting curve is set as four.

Fig. 8 presents the averaged positioning error of the rotational positioning model under the consideration of the different lengths of the rotating arm l. We see that the averaged positioning error in the measured room is minimized when $l = 10$ cm. Moreover, when the length of the rotating arm $l < 10$ cm, the shorter the rotating arm is, the higher the positioning error is (due to the limited space, the results for the case $l < 5$ cm is not presented in Fig. 8). This is mainly because a shorter rotating arm usually results in a smaller variation range of the power received by the PD, and thus the estimation error of the relative angle values (16) and (17) increases, and so does the positioning error. Therefore, if the measured area is too small for the proposed positioning system with a rotating arm 5 cm or more, other positioning devices need to be considered. In this sense, the proposed VLP system is more suitable for positioning in a medium-sized area, such as a small warehouse, or a nursing room. In the following simulations, we always let $l = 10$ cm.

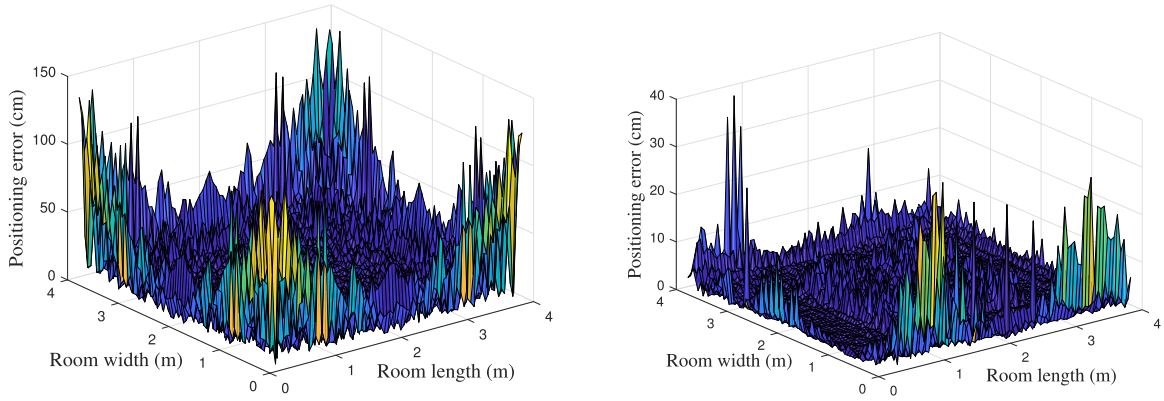

(a) without the hybrid positioning algorithm.

(b) with the hybrid positioning algorithm.

Fig. 10. Positioning error distribution with and without the hybrid positioning algorithm. (a) Without the hybrid positioning algorithm. (b) With the hybrid positioning algorithm.

Using the fitting data shown in Fig. 7, the distributions of positioning error in the measured room are presented in Fig. 9 for the case of line-of-sight (LOS) and in Fig. 10(a) for the NLOS case, respectively. From Fig. 9, we see that the positioning error of most locations in the measured room is below 10 cm in the LOS case.[4] By comparing Figs. 9 and 10(a), we see that there is an obvious gap in positioning error between the LOS and NLOS cases, and thus the effect of reflected path can be observed.

From Fig. 10(a), we also see that the closer the position of the PD is to the walls or the corners, the higher the positioning error is. Particularly, when the position is less than 1m away from the walls or the corners, the error becomes extremely large. Based on the simulation results, we found that the positioning error drops at the minimum 9.76 cm at the center of the room, and it reaches the maximum 137.96 cm near the corners. The averaged positioning error of the entire room is about 11.97 cm. Moreover, for 90% and 50% of the positions, the positioning error is less than 27 cm and 5 cm, respectively. Therefore, the width and the length of each wall or corner zones can be taken as 1 m and 3 meters, respectively (As shown in Fig. 3, $a = 1$ m and $b = 3$ m).

Fig. 10(b) presents the positioning error distribution of the proposed hybrid positioning algorithm. Compared to the results shown in Fig. 10(a), we see that by using the proposed hybrid positioning algorithm, the positioning error of the entire room drops dramatically. Particularly, within the wall or corner zones, the maximum error drops from 137.96 cm to 38.34 cm, and the averaged error decreases from 15.63 cm to 1.43 cm. Correspondingly, the averaged positioning error of the whole room decreases to 1.74 cm.

Fig. 11 provides the classification accuracy of the RF algorithm by considering the different numbers of the decision tree. We see that the accuracy increases with the number of the decision trees. Especially, after the number of the decision trees is no less than 99, the accuracy converges to about 95.5%.

[4]The positioning error near the central area is relatively high because when the position of the TN is close to the position of the LED projection point, the difference in power received by the PD for one rotation is very small, which will lead to a large error in the relative angle.

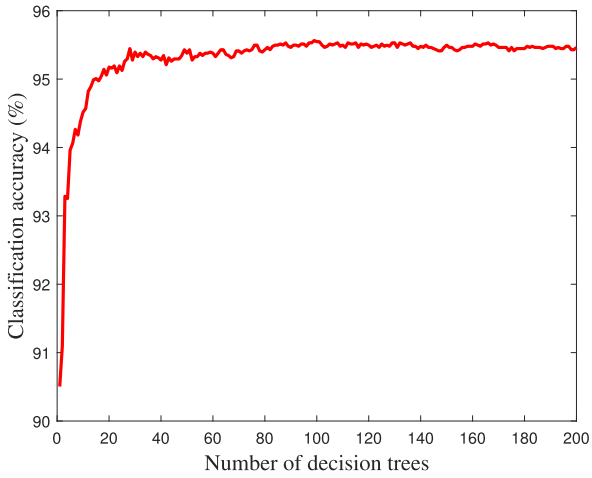

Fig. 11. Relationship between the accuracy of the RF classification algorithm and the number of decision trees.

Fig. 12 illustrates an example of clustering results using the DBSCAN algorithm. The sampled location $[0.6, 0.1]$ belongs to the wall or corner zone #1, and it is detected as a singular point since the estimated location drifts across the boundary of the zone. Therefore, by using the DBSCAN algorithm, the seven estimated coordinates of TN (defined as noise in this paper) that deviate from the true coordinates of TN will be removed, and the largest cluster which including the eight red cross points can be used to estimate the target location.

Fig. 13 provides the cumulative error function of the four wall or corner zones by using the rotatable positioning model with and without the proposed hybrid positioning algorithm. We see that by using the hybrid positioning algorithm, the positioning error is less than 3 cm in 90% of the wall or corner zones.

Finally, we compare the performance of the proposed hybrid ML positioning algorithm and the other ML algorithms in the Table III, in which the number of required LEDs and the average positioning error are compared for six investigated ML algorithms. We see that the DBSCAN algorithm [17] has the best

TABLE III
ACCURACY COMPARISON BETWEEN OUR PROPOSED ALGORITHM AND OTHER MACHINE LEARNING ALGORITHMS

ML algorithm	ANN [15]	CNN [16]	DBSCAN [17]	RR [18]	ELM [19]	Our proposed algorithm
Number of LEDs	4	81	25	9	4	1
Average accuracy (cm)	3.29	Not Provided	0.35	Not Provided	3.65	1.74

TABLE IV
PERFORMANCE COMPARISON BETWEEN OUR WORK AND OTHER EXISTING CAMERA-BASED VLP SYSTEMS WITH SINGLE LED

Scheme	Proposed in [6] (experiment)	Proposed in [22] (experiment)	Proposed in [23] (experiment)	Our work (simulation)
Time consumption (ms)	60	Not Provided	184	7983
Average accuracy (cm)	2.26	17.52	2.47	1.74
LED-Coverage Dimension	$1.8m\times1.8m\times3m$ 2D	$3m\times3m\times2m$ 2D	$6.8m\times2.7m\times2.7m$ 3D	$4m\times4m\times3.1m$ 2D

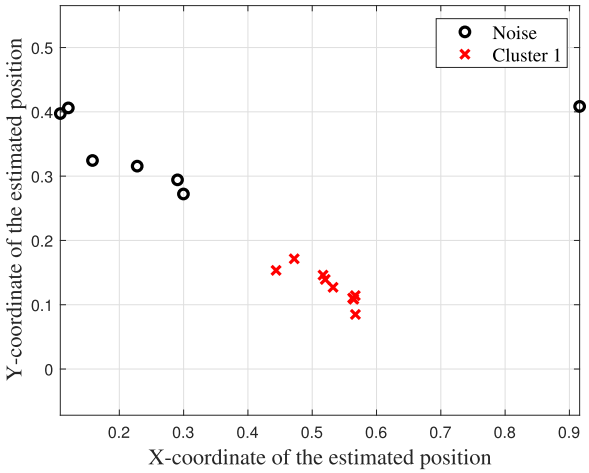

Fig. 12. An example of clustering results using the DBSCAN algorithm ($\varepsilon = 0.08$ m, $MinPts = 6$).

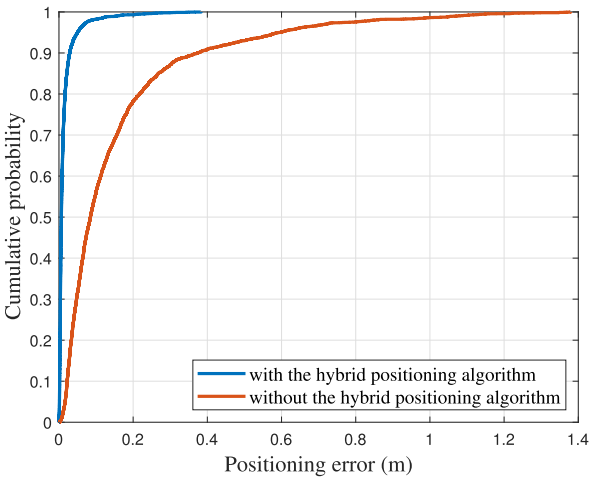

Fig. 13. Cumulative error function of the wall or corner zones using the rotatable positioning model with and without the proposed hybrid positioning algorithm.

positioning performance, but it requires 25 LEDs. Our proposed hybrid ML algorithm only needs the minimum number of LEDs. Moreover, compared to the ANN [15] and ELM [19] algorithms, it possesses much better positioning performance. Therefore, our proposed hybrid ML algorithm achieves a good trade-off between positioning accuracy and implementation cost, and it can be used as an alternative to high precision positioning algorithms for cost-sensitive applications.

Table IV shows the comparison between our work and other camera-based schemes with single LED in terms of time consumption, average accuracy, LED-coverage and dimension. It can be seen that the accuracy of our proposed system is the best. However, the benefit in accuracy comes at the expense of time consumption. Although the proposed positioning system can be accelerated in practice via optimized hardware design, it is more suitable for those indoor applications that are not sensitive to positioning delay. For example, when an elderly person with limited mobility seeks help in a nursing home, the proposed positioning system can be used to locate or track his/her movement trajectory at regular intervals. Moreover, a robot equipped with this positioning system can also be used in a small warehouse to detect changes in temperature or humidity at desired locations. Moreover, a robot equipped with this positioning system can also be used in a small warehouse to detect changes in temperature or humidity at desired locations.

Simulation results show that our proposed scheme works well in small rooms. However, if our proposed scheme is used in a very large room, there should be two concerns need to be addressed. Firstly, due to the acquisition of massive training data for machine learning, a very large room could pose a relatively high processing latency which is not conducive to the implementation of a real-time positioning system. Moreover, in a very large room equipped with single LED, the lighting power may be insufficient to provide both effective lighting and accurate positioning.

V. CONCLUSION

In this paper, a ML algorithm based VLP system with single-LED and single PD is proposed for indoor localization scenarios. In the VLP system, a rotatable positioning model is used to determine the target node's location in the interior area. Particularly, a hybrid ML-based positioning algorithm is proposed to improve the positioning accuracy near the walls or corners. Simulation results show that by using the rotatable positioning model in conjunction with the hybrid positioning algorithm, the positioning error of the entire room decreases significantly. Therefore, the proposed VLP algorithm is a promising solution for the indoor high-precision localization applications with low cost.

Algorithm 2: ELM Algorithm.

Inputs: Training sample set $(\mathbf{x}_i, \mathbf{y}_i), i = 1, \ldots, N$, number of hidden neurons L and activation function $g(\cdot)$.
1: Randomly generate $\boldsymbol{\omega}_i$ and $\mathbf{b}_i,\ i = 1, \ldots, L$;
2: Calculate $\mathbf{H}$ using (12);
3: Calculate $\hat{\boldsymbol{\beta}}$ using (13);
Outputs: Output the estimated weight $\hat{\boldsymbol{\beta}}$.

Algorithm 3: DBSCAN Algorithm.

Inputs: Sample set $D = [(x_1, y_1), (x_2, y_2), \ldots, (x_m, y_m)]$, neighborhood parameter $(\varepsilon, MinPts)$, definition the distance.
1: Initialize the core object collection $\Omega = \oslash$, number of clusters $k = 0$, unvisited sample collection $\Gamma = D$, and cluster partition $c = \oslash$;
2: Perform steps (a) and (b) for $j = 1, 2, \ldots, m$, to find all core objects;
a) Find the ε-neighborhood subsample set $N_\varepsilon(x_j, y_j)$ of the sample (x_j, y_j) by calculating the distance of definition.
b) If the number of subsample sets is greater than or equal to $MinPts$, add the samples (x_j, y_j) to the core object sample sets: $\Omega = \Omega \cup (x_j, y_j)$.
3: If $\Omega = \oslash$, the algorithm ends, otherwise go to step 4;
4: Randomly select a core object o in Ω, initialize the current cluster core object queue $\Omega_{cur} = \{o\}$, category number $k = k + 1$, current cluster sample set $C_k = \{o\}$, unvisited sample collection $\Gamma = \Gamma - \{o\}$;
5: If $\Omega_{cur} = \oslash$, generate cluster C_k, update the core object collection $\Omega = \Omega - C_k$, go to step 3;
6: Take out a core object o' in Ω_{cur}, find the ε-neighborhood subsample set $N_\varepsilon(o')$, let $\Delta = N_\varepsilon(o') \cap \Gamma$, update $C_k = C_k \cup \Delta,\ \Gamma = \Gamma - \Delta,$ $\Omega_{cur} = \Omega_{cur} \cup (\Delta \cap \Omega) - o'$, go to step 5;
Outputs: Cluster partition $c = \{C_1, C_2, \ldots, C_k\}$.

APPENDIX A
IMPLEMENTATION STEPS OF THE RF CLASSIFICATION ALGORITHM

The implementation steps of the RF classification algorithm are summarized as follows [33]:

Step 1: Randomly select p training samples from the original training set with replacement and generate q training sets after q selections;

Step 2: The q training sets selected in the first step above are used to train q decision tree models;

Step 3: These q decision trees can construct a random forest;

Step 4: The new test sequence is voted by q decision trees to produce the final classification result.

APPENDIX B
IMPLEMENTATION PROCESS OF THE ELM ALGORITHM

The implementation steps of training the ELM algorithm are as shown in Algorithm 2.

APPENDIX C
PROCEDURE OF THE DBSCAN ALGORITHM

The procedure of the DBSCAN algorithm is presented in Algorithm 3.

REFERENCES

[1] H. Yang, W.-D. Zhong, C. Chen, A. Alphones, and P. Du, "QoS-driven optimized design-based integrated visible light communication and positioning for indoor IoT networks," *IEEE Internet Things J.*, vol. 7, no. 1, pp. 269–283, Jan. 2020.

[2] H. Cheng, C. Xiao, Y. Ji, J. Ni, and T. Wang, "A single LED visible light positioning system based on geometric features and CMOS camera," *IEEE Photon. Technol. Lett.*, vol. 32, no. 17, pp. 1097–1100, Sep. 2020.

[3] Y.-C. Wu *et al.*, "Using linear interpolation to reduce the training samples for regression based visible light positioning system," *IEEE Photon. J.*, vol. 12, no. 2, Apr. 2020, Art. no. 7901305.

[4] A. H. A. Bakar, T. Glass, H. Y. Tee, F. Alam, and M. Legg, "Accurate visible light positioning using multiple-photodiode receiver and machine learning," *IEEE Trans. Instrum. Meas.*, vol. 70, pp. 1–12, 2021.

[5] Y. Liu, F. Wang, J. Ding, and N. Chi, "A single LED multi-reception indoor visible light position system based on power estimation-angle algorithm," in *Proc. Int. Symp. Intell. Signal Process. Commun. Syst.*, 2018, pp. 363–367.

[6] H. Li *et al.*, "A fast and high-accuracy real-time visible light positioning system based on single LED lamp with a beacon," *IEEE Photon. J.*, vol. 12, no. 6, Dec. 2020, Art. no. 7906512.

[7] S. Ma, Q. Liu, and P. C.-Y. Sheu, "Foglight: Visible light-enabled indoor localization system for low-power IoT devices," *IEEE Internet Things J.*, vol. 5, no. 1, pp. 175–185, Feb. 2018.

[8] Y. Hou, Y. Xue, C. Chen, and S. Xiao, "A RSS/AOA based indoor positioning system with a single LED lamp," in *Proc. Int. Conf. Wireless Commun. Signal Process.*, 2015, pp. 1–4.

[9] M. Katz and I. Ahmed, "Opportunities and challenges for visible light communications in 6G," in *Proc. 2nd 6G Wireless Summit*, 2020, pp. 1–5.

[10] X. Guo, F. Hu, N. R. Elikplim, and L. Li, "Indoor localization using visible light via two-layer fusion network," *IEEE Access*, vol. 7, pp. 16421–16430, 2019.

[11] Y. S. Eroglu, F. Erden, and I. Guvenc, "Adaptive Kalman tracking for indoor visible light positioning," in *Proc. IEEE Mil. Commun. Conf.*, 2019, pp. 331–336.

[12] S.-W. Ho, A. A. Saed, L. Lai, and C. W. Sung, "Coding and bounds for channel estimation in visible light communications and positioning," *IEEE J. Sel. Areas Commun.*, vol. 36, no. 1, pp. 34–44, Jan. 2018.

[13] H. Zheng, Z. Xu, C. Yu, and M. Gurusamy, "Asychronous visible light positioning system using FDMA and ID techniques," in *Proc. Conf. Lasers Electro-Opt. Pacific Rim*, 2017, pp. 1–4.

[14] Y.-A. Chen, Y.-T. Chang, Y.-C. Tseng, and W.-T. Chen, "A framework for simultaneous message broadcasting using CDMA-based visible light communications," *IEEE Sensors J.*, vol. 15, no. 12, pp. 6819–6827, Dec. 2015.

[15] S. Ni, F. Wang, S. Han, J. Pang, and S. You, "Two methods of accurate indoor positioning based on visible light communication system and artificial neural network," in *Proc. 18th Int. Conf. Opt. Commun. Netw.*, 2019, pp. 1–3.

[16] B. Zhou and R. Wichman, "Visible light-based robust positioning under detector orientation uncertainty: A gabor convolutional network-based approach extracting stable texture features," in *Proc. IEEE 30th Int. Workshop Mach. Learn. Signal Process.*, 2020, pp. 1–6.

[17] A. Gradim, P. Fonseca, L. N. Alves, and R. E. Mohamed, "On the usage of machine learning techniques to improve position accuracy in visible light positioning systems," in *Proc. 11th Int. Symp. Commun. Syst. Netw. Digital Signal Process.*, 2018, pp. 1–6.

[18] C.-Y. Hong *et al.*, "Angle-of-arrival (AOA) visible light positioning (VLP) system using solar cells with third-order regression and ridge regression algorithms," *IEEE Photon. J.*, vol. 12, no. 3, Jun. 2020, Art. no. 7902605.

[19] Y. Chen, W. Guan, J. Li, and H. Song, "Indoor real-time 3-D visible light positioning system using fingerprinting and extreme learning machine," *IEEE Access*, vol. 8, pp. 13875–13886, 2020.

[20] S.-H. Yang, E.-M. Jung, and S.-K. Han, "Indoor location estimation based on LED visible light communication using multiple optical receivers," *IEEE Commun. Lett.*, vol. 17, no. 9, pp. 1834–1837, Sep. 2013.

[21] S.-H. Yang, H.-S. Kim, Y.-H. Son, and S.-K. Han, "Three-dimensional visible light indoor localization using AOA and RSS with multiple optical receivers," *J. Lightw. Technol.*, vol. 32, no. 14, pp. 2480–2485, 2014.

[22] R. Zhang, W.-D. Zhong, Q. Kemao, and S. Zhang, "A single LED positioning system based on circle projection," *IEEE Photon. J.*, vol. 9, no. 4, Aug. 2017, Art. no. 7905209.

[23] L. Huang, S. Wen, Z. Yan, H. Song, S. Su, and W. Guan, "Single LED positioning scheme based on angle sensors in robotics," *Appl. Opt.*, vol. 60, no. 21, pp. 6275–6287, 2021.

[24] L. Li, P. Hu, C. Peng, J. Shen, Zhao, and Feng, "Epsilon: A visible light based positioning system," in *Proc. 11th USENIX Symp. Netw. Syst. Des. Implementation*, 2014, pp. 331–343.

[25] Y. Zhuang *et al.*, "A survey of positioning systems using visible LED lights," *IEEE Commun. Surv. Tuts.*, vol. 20, no. 3, pp. 1963–1988, Jul.-Sep. 2018.

[26] T. Komine and M. Nakagawa, "Fundamental analysis for visible-light communication system using LED lights," *IEEE Trans. Consum. Electron.*, vol. 50, no. 1, pp. 100–107, Feb. 2004.

[27] K. Lee, H. Park, and J. R. Barry, "Indoor channel characteristics for visible light communications," *IEEE Commun. Lett.*, vol. 15, no. 2, pp. 217–219, Feb. 2011.

[28] H. Schulze, "Frequency-domain simulation of the indoor wireless optical communication channel," *IEEE Trans. Commun.*, vol. 64, no. 6, pp. 2551–2562, Jun. 2016.

[29] W. Xu, J. Wang, H. Shen, H. Zhang, and X. You, "Indoor positioning for multiphotodiode device using visible-light communications," *IEEE Photon. J.*, vol. 8, no. 1, Feb. 2016, Art. no. 7900511.

[30] Y. Cai, W. Guan, Y. Wu, C. Xie, Y. Chen, and L. Fang, "Indoor high precision three-dimensional positioning system based on visible light communication using particle swarm optimization," *IEEE Photon. J.*, vol. 9, no. 6, Dec. 2017, Art. no. 7908120.

[31] S. Feng, X. Li, R. Zhang, M. Jiang, and L. Hanzo, "Hybrid positioning aided amorphous-cell assisted user-centric visible light downlink techniques," *IEEE Access*, vol. 4, pp. 2705–2713, 2016.

[32] X. Liu, D. Zou, N. Huang, and S. Zhang, "A comprehensive accuracy analysis of visible light positioning under shot noise," in *Proc. IEEE/CIC Int. Conf. Commun. China*, 2020, pp. 167–172.

[33] N. A. Maung Maung, B. Y. Lwi, and S. Thida, "An enhanced RSS fingerprinting-based wireless indoor positioning using random forest classifier," in *Proc. Int. Conf. Adv. Inf. Technol.*, 2020, pp. 59–63.

[34] X. Guo, S. Shao, N. Ansari, and A. Khreishah, "Indoor localization using visible light via fusion of multiple classifiers," *IEEE Photon. J.*, vol. 9, no. 6, Dec. 2017, Art. no. 7803716.

[35] L. Lian, S. Xia, S. Zhang, Q. Wu, and C. Jing, "Improved indoor positioning algorithm using KPCA and ELM," in *Proc. 11th Int. Conf. Wireless Commun. Signal Process.*, 2019, pp. 1–5.

[36] A. F. Khalifeh, N. AlFasfous, R. Theodory, S. Giha, and K. A. Darabkh, "On the effect of light emitting diodes positions on the performance of an indoor visible light communication system," in *Proc. IEEE Conf. Russian Young Researchers Elect. Electron. Eng.*, 2019, pp. 10–14.